High-resolution infrared spectroscopy of the $J=1$ H_2 pair in parahydrogen crystals

Y. Zhang, T. J. Byers,* M.-C. Chan,† T. Momose,‡ K. E. Kerr,§ D. P. Weliky,‖ and T. Oka
The Department of Chemistry, The Department of Physics, The Department of Astronomy and Astrophysics, and The Enrico Fermi Institute, The University of Chicago, Chicago, Illinois 60637
(Received 29 December 1997)

We have conducted high-resolution laser spectroscopic studies of the ortho-H_2 impurity-pair $Q_1(1)$ ($v=1\leftarrow 0$, $J=1\leftarrow 1$) transitions in solid para-H_2 with the ortho-H_2 concentration of $\leqslant 0.2\%$. Several hundred lines were observed in the frequency region between 4142.9 and 4150.3 cm^{-1}, with the linewidth of 7 to 200 MHz half width at half maximum. Except for the single-molecule $Q_1(1)$ transition located at 4146.5621 cm^{-1}, all transitions are due to the pairs and higher-order clusters of ortho-H_2. Using calculated relative intensities for spectral lines of nearest-neighbor (NN) pairs and next-nearest-neighbor (NNN) pair, and the accurate energy levels of the ground states by microwave spectroscopy [B. W. Statt, W. N. Hardy, and R. Jochemsen, Can. J. Phys. **58**, 1326 (1980)], we have assigned 180 spectral lines that are due to NN and NNN pairs, including both symmetric and antisymmetric excited states. The ground-state frequency-combination differences agree to within 0.001 cm^{-1}, the accuracy of the measurement. The agreement of the relative intensities and polarization dependences between the observed spectrum and the calculated spectrum is also satisfactory. The energy levels in the excited states obtained from the assignment demonstrate that the pair splitting due to the first- and second-order electric quadrupole-quadrupole (EQQ) interaction and the crystal-field interaction remains similar between the ground and excited states. Small and similar deviations from the ground state have been noted for the excited states of NN in-plane (IP), NN out-of-plane (OP), and NNN pairs. The widths of the observed spectral lines differ by more than an order of magnitude depending on the levels. We noticed that only the $F=2$, $M=0$ level, which has the highest energy among all the F,M components due to the EQQ interaction, has significant homogeneous broadening on the order of 100 MHz due to relaxation to the lower F,M levels. The inhomogeneous broadening due to the randomly distributed ortho-H_2 is approximately proportional to the difference in EQQ energy between the ground and excited F,M levels. These observations were useful in conducting spectral assignments. Complete energy level patterns for the six excited states: NN IP (s,a), NN OP (s,a), and NNN (s,a) pairs have been determined and discussed. A comprehensive analysis using the Hamiltonian is left for a future work. [S0163-1829(98)02325-X]

I. INTRODUCTION

Since the observation of the Raman spectrum of liquid hydrogen by McLennan and McLeod,[1] and the infrared spectrum of solid hydrogen by Allin, Hare, and MacDonald,[2] it has been well known that hydrogen molecules are rotating nearly freely in the condensed phase,[3] because of (a) the weak intermolecular interaction and the resulting large intermolecular distance, and (b) the nearly spherical charge distribution in the molecule. The total nuclear spin quantum number I, which specifies ortho ($I=1$) and para ($I=0$) spin modifications, is almost a rigorous good quantum number and the rotational angular momentum quantum number J is a good quantum number. At the liquid helium temperature where solid hydrogen samples have been studied, all para-H_2 molecules are in the $J=0$ level, and ortho-H_2 molecules are in the $J=1$ level. While para-H_2 in the $J=0$ level is spherically symmetric, and its interaction is isotropic, ortho-H_2 in the $J=1$ level is anisotropic. Sublevels of the latter with different magnetic quantum number M, which are degenerate in free space, are split in the anisotropic crystal field.[4] This splitting is very small (0.0071 cm^{-1}) for $J=1$ impurity surrounded by $J=0$ H_2 and its direct measurement has been reported only recently.[5] However, the splitting of the sublevels becomes much larger and amounts to several wave numbers when two $J=1$ H_2 molecules are close to each other to form a pair. It is this type of splitting that we discuss in this paper.

The large interaction between $J=1$ pair molecules was suspected in the early observation of the anomalous specific heat[6,7] and the anomalous temperature variation in the width of the $J=1$ H_2 NMR signal.[8–10] Nakamura,[11] in a paper which ''marks the beginning of the modern microscopic theory of the solid hydrogen''[4] located the origin of the interaction as the electric quadrupole-quadrupole interaction between the $J=1$ H_2 and, using the experimental value of the H_2 quadrupole moment given by Harrick and Ramsey,[12] explained the major part of the specific heat anomalies reported by Hill and Ricketson.[13] The validity of Nakamura's interpretation was further evidenced by a neutron-diffraction experiment[14] and NMR spectroscopy.[15] Nakamura's theory was greatly extended by Harris,[16] who considered finer intermolecular interactions and phonon renormalization, paving the way to his later spectroscopic analysis.

A direct observation of the split energy levels of the $J=1$ pair was reported by Silvera, Hardy, and McTague[17] using Raman spectroscopy. The splitting was also observed by Boggs and Welsh[18] in the infrared region as a simultaneous transition with the $Q_1(0)$ ($v=1\leftarrow 0$, $J=0\leftarrow 0$) pure vibrational transition. The time variations in the intensities of pair spectrum in NMR (Ref. 19) and infrared[18] were used to study quantum diffusion in solid hydrogen. Experimental in-

formation on the $J=1$ pair splitting made a quantum jump in 1975 when Hardy and Berlinsky[20] observed the high-resolution microwave spectrum (hereafter called the pair spectrum) between the split levels of the ''impurity'' $J=1$ H_2 pair in nearly pure para-H_2 crystals, using a calorimetric method. This and subsequent observations[21,22] have revealed extremely sharp spectral lines [$\Delta\nu \approx 1.5-40$ MHz half width at half maximum (HWHM)] and fine structure demonstrating intricate nature of the intermolecular interactions of the $J=1$ H_2 pair embedded in the $J=0$ H_2 crystal and leading to extensive theoretical studies.[23,24] The relaxation mechanism relating to line width[25] and the temperature and pressure dependence of the spectrum[26] were also studied. The treatment of the present paper borrows heavily from the understanding and energy information obtained from the microwave works.

With the advent of new techniques in infrared spectroscopy, the hydrogen pair spectrum came to be studied in the infrared region. The $v=1\leftarrow 0$ spectrum of the pair has been reported using Fourier-transform spectroscopy in medium resolution[27] and in high resolution ($\Delta\nu \approx 0.011$ cm^{-1}).[28] Laser infrared spectroscopy[29] has demonstrated that the fine structure of the vibrational pair spectrum can be observed with the linewidth comparable to those of the microwave spectrum resulting in the absolute resolution of $\Delta\nu/\nu \sim 10^{-7}$. Since in this case the pair levels in the excited state are also split into 18 components, the number of spectral lines is greatly increased. Several hundred lines were observed in the region between 4142.9 and 4150.3 cm^{-1} with the linewidth of 7 to 200 MHz HWHM, centered at 4146.5621 cm^{-1}, the single-molecule $Q_1(1)$ ($v=1\leftarrow 0$, $J=1\leftarrow 1$) transition frequency. The present paper reports our recent observations and an analysis of these structures.

II. EXPERIMENT

The complete spectrum has been recorded several times, three times in the original scans with different ortho-H_2 concentrations (0.2 and 0.06 %),[29] and several times later when we studied spectroscopically the γ-ray-irradiated para-H_2 crystals (0.2% ortho-H_2).[30] These scans were done with a difference-frequency (DF) laser spectrometer. Recently we rescanned the region with a color-center laser (CCL) spectrometer. The CCL system allows better accuracy in frequency measurement, higher sensitivity, and higher resolution compared to the DF system. Consequently, many previously unseen transitions were observed and previously overlapped transitions were resolved. More importantly, because of the much higher accuracy in frequency measurement enabled by the CCL system, assignments can be done with confidence using combination differences in the central region of the spectrum, where spectral lines are very much congested. In total two crystals (0.2% ortho-H_2) were measured with the CCL system. The method of crystal preparation has changed in the intervening eight years. However, the observed spectra are very consistent with each other (within 0.0005 cm^{-1}) if a scale factor is allowed for the splitting of the F,M levels, indicating the reliability of the observed spectrum. This linear scale factor results from slightly different temperatures (a few K) at which the crystals were made and will be discussed below and later in Sec. VI A.

Para-H_2 crystals were grown in a copper cell 2 cm in diameter and 11.5 cm in length, which were sealed by wedged (0.5°) sapphire windows with indium gaskets and mounted in a commercial helium Dewar. The sapphire windows were cut with their c axis normal to the surface so that accurate polarization dependence of the spectral lines can be observed. Para-H_2 gas was produced by liquefying high-purity hydrogen gas from a hydrogen purifier into a column of APACHI nickel silicate catalyst placed above the liquid helium surface in a commercial Dewar at 14 to 20 K. The liquid H_2 was kept for a few hours and extracted at a temperature controlled by the height of the catalyst container from the helium surface. Lower temperature gives lower ortho concentration. After the conversion, the para-H_2 gas was introduced into the cylindrical sample cell through a $\frac{1}{16}$ in. o.d. stainless steel tube with the rate that kept the temperature of the cell at about 11 K. The temperature was measured by a Ge resistance temperature sensor mounted on the cell. The hydrogen condensed directly from gas to solid and the crystal grew radially inward from the wall. After the cell was filled, the temperature was brought down slowly to around 5 K. The crystal did not simply settle into the equilibrium structure at 5 K. Since the crystal was attached to the copper wall of the cell and the thermal expansion of the crystal is higher than that of copper, the crystal was under negative pressure. This resulted in a crystal with a slightly larger lattice constant than that of a freestanding crystal at 2.1 K used in the microwave experiment.[21,22] Therefore, the pair splitting is slightly smaller than that in the microwave experiment. Since the major cause of the splitting, the electric quadrupole-quadrupole (EQQ) interaction, is inversely proportional to the fifth power of the intermolecular distance R, the variation of the pair splitting is approximately proportional to the variation of R. Because of the slight difference in temperatures at which different crystals were made, the frequencies of transitions vary as much as 0.007 cm^{-1} from crystal to crystal for levels far from the center of the EQQ splitting. However, we see our measurement of each crystal is consistent when a scaling factor taking into account the variation in crystal size is applied. A set of frequency data for a particular crystal (0.2% ortho-H_2) is used in this paper. Since the molar volume of para-H_2 crystal varies little from 11 to 5 K,[31] a crystal with little stress and without breakage is obtained by this method. The temperature at which the crystal is made is crucial to the quality of the final crystal. Higher temperature gives a more transparent crystal to begin with, but which is more likely to break as the temperature is lowered. Crystal made at lower temperature is more stable for lowering its temperature, but is less transparent probably because of the decreased tunneling of the molecules during crystallization. The growth of large single crystals by condensing directly from gas to solid has also been reported by the Kharkov group.[32] While our crystal was not a complete single crystal because of our method of growing it from a cylindrically shaped wall, the sharpness, purity, and reproducibility of our high-resolution spectra[33,34] imply that the crystal had a good hexagonal close packed (hcp) lattice at least locally where the laser radiation (diameter ≈ 1 mm) probed the sample. There is usually a bubble of about 4 mm in diameter in the center of the cell, but we have at least a few millimeters of transparent sample for laser spectroscopy.

A more detailed description of the crystal preparation can be found in Kerr's thesis.[35]

The commercial color center laser is pumped by 2 W of the 647.1-nm radiation from a Kr^+ laser. The output power is about 10 mW in the region of interest. The free-running frequency jitter is 3 MHz. A tone burst technique[36] is employed in this system to improve the sensitivity. A CdTe electro-optic modulator in the path of the laser beam generates about 25% side bands from the radiation for rf frequency between 6 and 120 MHz. The side bands are switched on and off at a frequency of 30 kHz and the signal is detected by an InSb detector followed by a lock-in amplifier. The effect of the amplitude noise of the color center laser is minimized by splitting the beam and using the $A-B$ noise subtraction technique. The modulation gives spectral lines, the second derivative shape, and emphasizes sharp spectral features at the expense of broad ones. The sensitivity is typically $\Delta I/I \sim 5 \times 10^{-4}$. A temperature-stabilized étalon with a free spectral range of 150 MHz is utilized to generate wave number markers on the scans. Together with a NO_2 reference gas,[37] the frequency can be determined within 0.0002 cm^{-1} during one normal scan spanning 0.09 cm^{-1}. For a much more detailed description of the spectrometer, consult Weliky's thesis.[38]

For the crystal from which our final data are taken, we scanned the region with five different tone-burst side band frequencies (6.65, 13.05, 28.05, 60.05, and 120.05 MHz) using the color center laser with both perpendicular and parallel polarization of the laser radiation with respect to the c axis of the crystal. Tone burst modulation with higher frequency helps us observe broad lines near the outer edge of the scanned region, whose linewidth is on the order of 100 MHz, while the lower-frequency modulation allows better resolution for the congested sharp transitions in the center region.

III. THEORETICAL BACKGROUND

A. Single molecule $Q_1(1)$ transition

At 4146.5621 cm^{-1}, in the middle of the thicket of lines, is the single-molecule $Q_1(1)$ transition, which is by far the strongest among all the observed lines. It is infrared active through the quadrupole-induced-dipole mechanism, where the quadrupole moment of a $J=1$ molecule induces dipole moments on the surrounding para-H_2 molecules and these many-body dipole moments interact with the radiation to cause the central ortho-H_2 to be excited to the $v=1$ state. Direct quadrupolar transition is many orders of magnitude smaller. This mechanism was initially worked out by Sears and Van Kranendonk,[39] who showed that in the hcp lattice of solid para-H_2, the transition is allowed only with radiation whose electric field is perpendicular to the c axis of the crystal, and the selection rule for the transition is $\Delta M = \pm 2$. Here M is the magnetic quantum number, i.e., the projection of the rotational angular momentum J along the c axis. Experimentally the two transitions $M=1 \leftarrow M=-1$ and $M=-1 \leftarrow M=1$ are observed at the same frequency because the $M=\pm 1$ levels are degenerate in the hcp lattice due to the threefold symmetry axis C_3. All the other features observed in our experiment are due to the ortho-H_2 pair with a variety of relative positions and to higher ortho clusters randomly distributed in the lattice structure. For the low ortho concentration in our samples ($\leqslant 0.2\%$) we expect that the pair transitions dominate these lines. In this paper, we restrict ourselves to the study of the nearest-neighbor (NN) and next-nearest-neighbor (NNN) ortho-H_2 pair transitions.

B. Pair splitting

The complexity of the pair spectrum is caused by the interactions between a pair of $J=1$ H_2 molecules and their surrounding $J=0$ para-H_2 molecules. Since there are three sublevels for one $J=1$ molecule with $M=0,\pm 1$, a pair of ortho-H_2 has nine sublevels. These nine sublevels would be degenerate if we were to consider two noninteracting molecules in free space but they are split because of intermolecular interaction between the two and the crystal-field interaction. For a pair of $J=1$ H_2 there are different relative positions in the lattice. There are in-plane (IP) and out-of-plane (OP) pairs for NN pair, while there is only one kind of NNN pair. In addition, the $v=1$ excitation can be on either molecule of the pair, causing an additional degree of freedom. In total, there are $9\times 9\times 2\times 2=324$ possible transitions for the NN pair, and $9\times 9\times 2=162$ for the NNN pair. Of course, only infrared active ones are observable, but because of the lowered symmetry due to the presence of the ortho-H_2 pair, many transitions are infrared active.

Various interactions which cause the splitting of the nine levels in the ground vibrational state of the $J=1$ pair were discussed by Harris, Berlinsky, and Hardy.[21,23] A schematic hierarchy of the splitting is shown in Fig. 1. Apart from the isotropic dispersion interaction (which amounts to about 25 cm^{-1},[40] but does not contribute to the splitting), the largest interaction between the $J=1$ molecules is the EQQ interaction[11] with the Hamiltonian

$$H_{\mathrm{EQQ}}=\sqrt{70}\,\frac{Q_1Q_2}{R_{12}^5}\sum_m C(224;m\bar{m}0)C_{2m}(\boldsymbol{\omega}_1)C_{2\bar{m}}(\boldsymbol{\omega}_2), \tag{1}$$

where $C(224;m\bar{m}0)$ are Clebsch-Gordan coefficients, $C_{2m}(\boldsymbol{\omega}_i)$ are Racah spherical harmonics of the ith molecule ($i=1,2$) with angle variable $\boldsymbol{\omega}_i$ with respect to the pair axis, and Q_i ($i=1,2$) are their quadrupole moments. This interaction splits the ninefold degenerate states into four levels with energies 6Γ, Γ, 0, and -4Γ where the EQQ splitting parameter $\Gamma \equiv 6Q^2/25R^5$ is 0.576 cm^{-1} for the NN pair[21] and 0.116 cm^{-1} for the NNN pair[22] in the ground vibrational state. The eigenfunction for H_{EQQ} are given by bipolar spherical harmonics

$$|F,M\rangle=\sum_{m,n} C(11F;mnM)|1m\rangle|1n\rangle, \tag{2}$$

with the total rotational angular momentum quantum number F and its projection along the pair axis M, where the first and the second eigenfunction on the right-hand side represent rotational state $|JM\rangle$ of the first and the second $J=1$ H_2, respectively. H_{EQQ} shifts and splits the five substates with $F=2$ into three levels with $M=0,\pm 1,\pm 2$ while the four states with $F=1$ and 0 are unaffected and stay degenerate. This degeneracy is lifted by other anisotropic interactions such as second-order EQQ interaction, dispersion, and induction.[41] However, the cylindrically symmetric (CS) interactions between the pair molecules leave the $\pm M$ levels

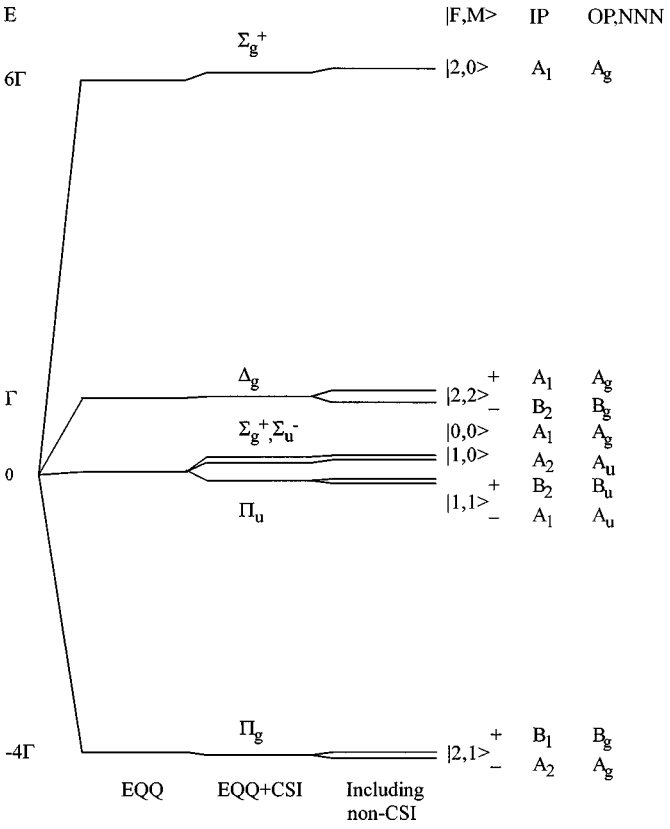

FIG. 1. The energy diagram of a pair of ortho-H_2 molecules in solid para-H_2 crystal and the symmetry of each level. Levels are labeled by the total angular momentum of the pair F and its projection onto the interpair axis M. The unit for energy is the electric quadrupole-quadrupole (EQQ) interaction splitting parameter $\Gamma \equiv 6Q^2/25R^5$, where Q is the quadrupole moment of the hydrogen, and R is the intermolecular distance. If only the EQQ interaction is considered the nine states split into four levels. Cylindrically symmetric (CS) interactions split the four $F=0$ and 1 states into three levels while maintaining the degeneracy of the $|11\rangle_{\pm}$ states. Noncylindrically symmetric (non-CS) interactions split all the nine levels. The symmetry is labeled for each level for a pair of ortho-H_2 in the free space (above ''EQQ+CSI'' in the figure) and three types of pairs in solid para-H_2: nearest-neighbor in-plane (IP), out-of-plane (OP), and next-nearest neighbor (NNN).

doubly degenerate. These degeneracies are lifted by noncylindrically symmetric (non-CS) interactions between the $J=1$ H_2 of the pair and the surrounding $J=0$ H_2. Since there still remains a plane of symmetry, the split states with $M \neq 0$ are expressed by

$$|F,M\rangle_{\pm} = \frac{|F,M\rangle \pm |F,-M\rangle}{\sqrt{2}}, \tag{3}$$

for $M>0$, where the $\pm$ represent eigenfunctions symmetric or antisymmetric with respect to the plane symmetry. The two interactions CS and non-CS also mix the nine $|F,M\rangle_{\pm}$ levels with the same symmetry (see Sec. III C), but these mixings are small and neglected in the $|F,M\rangle_{\pm}$ labels of the levels in Fig. 1 and in the theoretical calculation of the intensities.

The pair level pattern in the vibrationally excited state has an additional complication because the vibrational excitation (vibron) may be on either of the two molecules of the pair.[28,29] This leads to symmetric $|s\rangle$ and antisymmetric $|a\rangle$ vibrational eigenstates

$$\begin{matrix} |s\rangle \\ |a\rangle \end{matrix} = \frac{|v_1=1\rangle|v_2=0\rangle \pm |v_1=0\rangle|v_2=1\rangle}{\sqrt{2}}, \tag{4}$$

which are multiplied to $|FM\rangle_{\pm}$ to give the overall eigenfunctions. The energy difference between the s and a states is given by twice the vibron hopping frequency

$$v_h = \left\langle 10 \left| \frac{\partial^2 V}{\partial q_1 \partial q_2} q_1 q_2 \right| 01 \right\rangle = \frac{1}{2} \frac{\partial^2 V}{\partial q_1 \partial q_2}, \tag{5}$$

where V is the intermolecular potential in cm^{-1} and q_1 and q_2 are dimensionless vibrational coordinates of H_2 such that $\langle v|q|v-1\rangle = \sqrt{v/2}$. Since $V \approx -25\ \mathrm{cm}^{-1}$, $v_h \approx \kappa^2 V$,[42] where $\kappa \approx 10^{-1}$ is the Born-Oppenheimer constant, v_h is expected to be on the order of $-0.25\ \mathrm{cm}^{-1}$ and the antisymmetric level is higher than the symmetric level. Van Kranendonk[4] uses notation $\varepsilon' \equiv -\partial^2 V/\partial q_1 \partial q_2$ and $\varepsilon' = 0.41\ \mathrm{cm}^{-1}$, corresponding to $v_h = -0.21\ \mathrm{cm}^{-1}$, while Steinhoff *et al.*[28] gave $v_h = -0.29\ \mathrm{cm}^{-1}$. Since the equilibrium intermolecular distance in the crystal 3.783 Å (Ref. 31) is much higher than the equilibrium distance of the intermolecular potential 3.36 Å,[40,43] and is even higher than the inflexion point[4] 3.73 Å, molecules sense mostly the attractive part of the intermolecular potential due to the R^{-6} dispersion term. Thus, the hopping frequency is expected to scale by $\frac{1}{8}$ in going from NN to NNN pairs. We find that this is not the case and the scaling factor is $\frac{1}{3.3}$, indicating that the Raman-type hopping processes using nonresonant $J=0$ H_2 as stepping stones play an important role. This will be discussed in a separate paper.[44]

C. Symmetry, selection rules

A detailed theory of the vibration-rotational transitions of the $J=1$ H_2 pair will be published separately.[45] Here we summarize useful results without proof. First we consider a pair of nearly freely rotating $J=1$ H_2 without surrounding $J=0$ H_2. This system has cylindrical symmetry and the center of inversion, and the symmetry of the $|F,M\rangle$ states can be expressed by irreducible representations of the $D_{\infty h}$ point group[46] as shown in Fig. 1. The states are gerade g or ungerade u depending on whether F is even or odd and $M=0,\pm 1,\pm 2$ correspond to the Σ, Π, and Δ states, respectively. Since the H_2 molecule as a whole is regarded as a boson, g and u relate to $+$ and $-$, respectively, for the Σ states. We see that the only mixing due to the CS interaction is between $|2,0\rangle$ and $|0,0\rangle$. If we choose the z axis along the pair axis, the symmetries of the components of the transition dipole moment are $(\mu_x,\mu_y) \subset \Pi_u$, $\mu_z \subset \Sigma_u^+$. The selection rules are $\Delta F = \pm 1$ and $\Delta M = \pm 1$ for (μ_x,μ_y) and $\Delta M = 0$ for μ_z, the latter only for $M \neq 0$.

When the surrounding $J=0$ H_2 are also considered, the cylindrical symmetry is broken and the symmetry of the system is lowered (Fig. 2). The coordinate axes are chosen such that the z axis is along the pair axis and the y axis is the axis of C_2 rotation, then the symmetry of the IP pair system is C_{2v} with symmetry operations $\{E,\ C_2(y),\ \sigma(yz),$ and

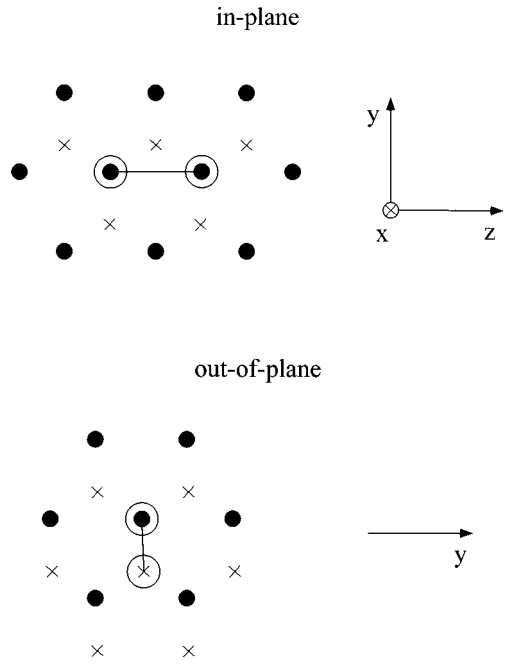

FIG. 2. Lattice configurations of nearest-neighbor in-plane and out-of-plane ortho-H_2 pairs, and the corresponding symmetry axes. Circles and crosses indicate two consecutive hexagonal planes in the hcp lattice of the para-H_2 crystal. Circled molecules are the ortho pair, while the others are the surrounding para-H_2 molecules.

$\sigma(xy)\}$, while that of OP and NNN pair system is C_{2h} with symmetry operations $\{E,\ C_2(y),\ i,$ and $\sigma(xz)\}$.[46] Irreducible representations of the levels are given in Fig. 1. Levels with the same symmetry are mixed by the non-CS crystal field interaction. For example, $|2,0\rangle$, $|2,2\rangle_+$, $|0,0\rangle$, and $|1,1\rangle_-$ belonging to A_1, are mixed for the IP pair, while $|2,0\rangle$, $|2,2\rangle_+$, $|0,0\rangle$, and $|2,1\rangle_-$ belonging to A_g are mixed for OP and NNN pairs. Symmetries of pair levels in the symmetric and antisymmetric excited vibrational states are obtained by multiplying A_1 and B_1 (for IP), and A_g and B_u (for OP and NNN), respectively, to the symmetry of the ground-state pair levels. Selection rules are obtained from the symmetry of components of the dipole moment parallel and perpendicular to the crystal c axis $\mu_\parallel=\mu_x\subset B_2$, $\mu_\perp=\mu_y\subset A_1$, and $\mu_z\subset B_1$ for IP pair and $\mu_\parallel=(\mu_x,\mu_z)\subset B_u$, $\mu_\perp=(\mu_x,\mu_z)\subset B_u$, and $\mu_y\subset A_u$ for OP and NNN pairs. For the latter pairs, the inversion symmetry is preserved and the selection rules are simply

$$g\leftrightarrow u \tag{6}$$

and

$$\Delta F=\pm 1. \tag{7}$$

For IP pair, where the center of symmetry no longer exists, the rules are more complicated. Anyhow, all of the observed transitions follow selection rules

$$\Gamma_i\otimes\Gamma_f\supset\Gamma_{\mu_\alpha}, \tag{8}$$

where $\Gamma_i,\Gamma_f,\Gamma_{\mu_\alpha}$ are irreducible representations of the initial and final states of the transition and μ_α is the component of the transition dipole moment. Not all of the transitions allowed by these rules were observed. For example, weak transitions induced by the small mixings of $|F,M\rangle_\pm$ states due to CS and non-CS interactions were not observed.

D. Relative intensities

Theoretical relative intensities of the pair transitions were very useful for their assignments. They were calculated[45] using the basis sets $|v\rangle|F,M\rangle_\pm$ $(v=0,s,a)$ and spherical components $(N=0,\pm 1)$ of quadrupole-induced dipole moment operators of molecule 1:

$$\mu_N^1=\sqrt{35}Q_1\sum_{k\neq 1}\sum_{m,n}\frac{\alpha_k}{R_{1k}^4}C(321;mnN)C_{2n}(\mathbf{\Omega}_1)C_{3m}(\mathbf{\Omega}_{1k}), \tag{9}$$

and the same expression with 1 replaced by 2, and

$$\begin{aligned}\overline{\mu_N^1}=&-\frac{5}{3}\sqrt{14}\,\frac{Q_1\gamma_2}{R_{12}^4}\sum_{m,n}C(211;m,N-m,N)\\&\times C(321;N-m-n,n,N-m)\\&\times C_{2n}(\mathbf{\Omega}_1)C_{2m}(\mathbf{\Omega}_2)C_{3,N-m-n}(\mathbf{\Omega}_{12}),\end{aligned} \tag{10}$$

and the same expression with 1 and 2 interchanged, where $\alpha=(2\alpha_\perp+\alpha_\parallel)/3$, and $\gamma=\alpha_\parallel-\alpha_\perp$ are the isotropic and anisotropic polarizability of H_2, respectively. $\mathbf{\Omega}_i$ and $\mathbf{\Omega}_{ik}$ are angle variables of molecule i and the direction $i\rightarrow k$ with respect to the crystal axis. The operator in Eq. (9) represents the sum of dipole moments induced in the surrounding molecules k (including 2) through their isotropic polarizabilities by the quadrupolar field of molecule 1, and the operator in Eq. (10) represents the dipole moment induced in molecule 2 through its anisotropic polarizability γ_2. Intensities calculated from $|\langle f|\mu_N^1+\mu_N^2|i\rangle|^2$ using Eq. (9) give terms that are proportional to the squares of $\alpha Q_{10}S_{33}^4$ and $\alpha_{10}Q$, while the intensities from $|\langle f|\overline{\mu_N^1}+\overline{\mu_N^2}|i\rangle|^2$ using Eq. (10) are proportional to the squares of $Q_{10}\gamma\pm Q\gamma_{10}$ ($\pm$ for $v=s$ and a, respectively), where $Q_{10}\equiv\langle 1|Q|0\rangle$, $\alpha_{10}\equiv\langle 1|\alpha|0\rangle$, and $\gamma_{10}\equiv\langle 1|\gamma|0\rangle$ are off-diagonal vibrational matrix elements of the respective quantities, and $S_{33}^4\equiv\Sigma_k(R_0/R_{1k})^4C_{33}(\Omega_{1k})=-0.391$ is a crystal sum. $N=0$ gives intensities when the polarization of the electric field of the laser radiation is parallel to the crystal c axis while $N=\pm 1$ gives intensities for the perpendicular polarization. The theoretical intensities are given in Fig. 3 as a computer-generated stick diagram. They are also shown below the observed spectral lines collected in Fig. 4.

E. Linewidths

Another observed characteristic of the individual spectral line that helped our assignment of the complicated spectrum is the linewidth. It is noted in Fig. 4 that widths of spectral lines vary widely depending on transitions. Since the tone-burst modulation method records higher intensities for narrower lines, we should take into account the linewidths in comparing relative intensities.

Although the method of our crystal preparation is less sophisticated than that of Hardy *et al.*[20,21] and our transition energies are higher by more than three orders of magnitude, we find that there exists a correlation between the linewidths of the infrared spectrum and the microwave spectrum. The

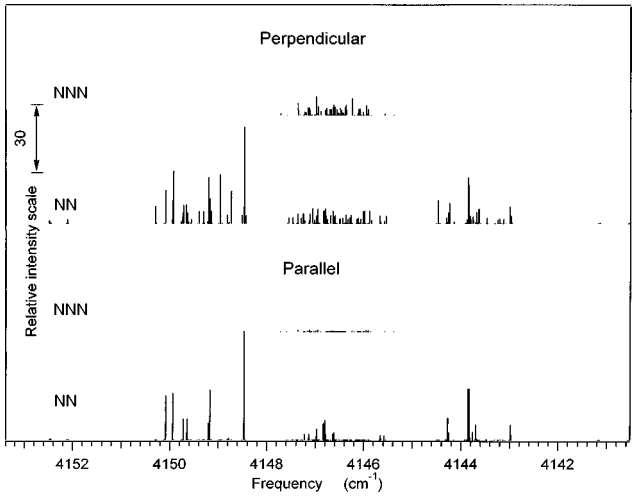

FIG. 3. Computer-generated stick diagram of the nearest-neighbor and next-nearest-neighbor pair transitions. Frequency is calculated from energy diagrams in Fig. 5. Calculated intensities for laser radiation field of both polarizations with respect to the c axis of the hcp lattice of the crystal are shown. For each polarization, the upper and lower stick diagrams refer to the NNN and NN pairs, respectively. The scale of the relative intensity is consistent with those of Fig. 4.

sharpest linewidth we observed is 7.8 MHz HWHM. This suggests that the linewidth resulting from vibrations such as T_1 vibron-phonon relaxation and T_2 vibron dephasing is not high. The energy of vibron 4150 cm^{-1} is nearly two orders of magnitude higher than the crystal Debye temperature[31] 70 cm^{-1}, and both T_1 and T_2 relaxations are expected to be very slow.[47–49] At the ortho concentrations of 0.2 and 0.06 % used in our experiment, the mean interpair distance is $\approx 35R_0$ and $78R_0$, respectively, and vibrons are well localized on the pairs. Overall, as far as the linewidths are concerned, we can ignore complications due to the vibrational excitation. The relaxation between the symmetric and antisymmetric excitations requires vibrational operators and is expected to be much slower than the relaxation between pair levels.

The linewidth of the microwave pair spectrum was studied experimentally[21,22] and theoretically[25] by Statt, Hardy, and Jochemsen. They observed that the linewidths vary greatly depending on the transition. For example, the linewidths for the $|1,1\rangle_{\pm} \leftarrow |2,1\rangle_{\mp}$ transitions were 13 MHz, one half of those for the $|1,1\rangle_{\pm} \leftarrow |2,1\rangle_{\pm}$ transitions although they appear in the same frequency region. Such variations of linewidths have also been noted in our infrared spectrum and give us an additional guide for spectral assignment. The infrared spectrum includes the Q-type transitions $|F,M\rangle \leftarrow |F,M\rangle$, which do not exist in a microwave spectrum. They were found to be very sharp as shown, for example, by line 117:IP-$s|1,1\rangle_- \leftarrow |1,1\rangle_-$ in Fig. 4. The same phenomenon was observed in HD and D_2 impurity spectra and explained by Weliky *et al.*[50] The levels with same quantum numbers in the excited and the ground state tend to be shifted similarly due to the presence of impurities and thus their differences are not much affected. Q-type transition $|2,0\rangle \leftarrow |2,0\rangle$ is the only exception for this because of a large homogeneous broadening. This will be discussed more fully later in Sec. VI C.

IV. ASSIGNMENT

The final assignment of the complicated spectrum was based on the method of ground-state combination difference using the accurately determined ground-state energy levels reported by Hardy and his collaborators.[20–23,25,26] During this procedure we noted that the ground-state energy values in our crystals are consistent with those by Statt, Hardy, and Jochemsen[22] within the accuracy of measurements (≈ 10 MHz) except for the scaling factor mentioned earlier and will be addressed later in Sec. VI A. Since the symmetry of the system is not very high, there are plenty of allowed transitions as discussed in Sec. III C and there was no shortage of ground-state combination differences. Thus, some energy values that are missing in the microwave work, such as IP $|1,1\rangle_{\pm}$ levels and the OP $|0,0\rangle$ level were readily filled using the infrared result. This assignment procedure is qualitatively different from and less satisfactory than the traditional method in which energy levels from an interaction Hamiltonian with suitable molecular constants are used. We abandoned this latter approach in view of the facts that (a) even for the simpler ground state, the extensive analysis by Harris *et al.*[23] did not explain all the levels and (b) our attempt to develop such calculation for the $J=6-J=1$ pair interaction ran into difficulty. The assignment based on the ground-state combination difference is also used in gaseous spectroscopy when the analysis of the excited state is prohibitively difficult as in the case of $C_2H_3^+$.[51,52]

The assignment of the transitions by the NN pairs proceeded as follows. Here we were helped by the work by Steinhoff *et al.*[28] especially for taking into account the splitting between the symmetric and antisymmetric states, although our final assignments differ from theirs considerably in detail. We first simply scaled the ground-state splitting by Γ_s/Γ_0 or Γ_a/Γ_0 to approximate the pair splitting for the symmetric and antisymmetric $v=1$ vibrational states, respectively. This gave a reasonable first approximation for the F,M splitting since the first-order EQQ interaction is the dominant cause for the splitting. The values of Γ_0 were given by Hardy *et al.*[21] to be 0.576 07 cm^{-1} for IP pair and 0.575 26 cm^{-1} for OP pair. Γ_s and Γ_a for the excited states were estimated by assigning some of the more prominent spectral lines from frequency, linewidth, intensity, and polarization dependence. For example, the strong sharp line at 4148.4704 cm^{-1} was assigned the OP-s $11_+ \leftarrow 21_-$ transition and the line at 4143.8595 cm^{-1} was assigned to be the OP-s $21_+ \leftarrow 11_-$. From the ground-state splitting of 2.210 85 cm^{-1} between 21_- and 11_- levels given by microwave work, splitting between the OP-s 11_+ and 21_+ levels was calculated to be 2.400 05 cm^{-1}. Comparing this value with the corresponding ground-state splitting of 2.138 05 cm^{-1} given by microwave work, the scaling for OP-s pair was calculated to be $\Gamma_s/\Gamma_0 = 1.122\,54$. This increase is mainly due to the 10.7% increase of the quadrupole moment of H_2 from 0.4853 to 0.5370 a.u. due to the vibrational excitation.[53] The scaling factors for other pair states were obtained similarly. In order to fill the IP $11_{\pm}$ levels and OP 00 levels that are missing in the microwave result, we assumed that in the first approximation the scaling of F,M

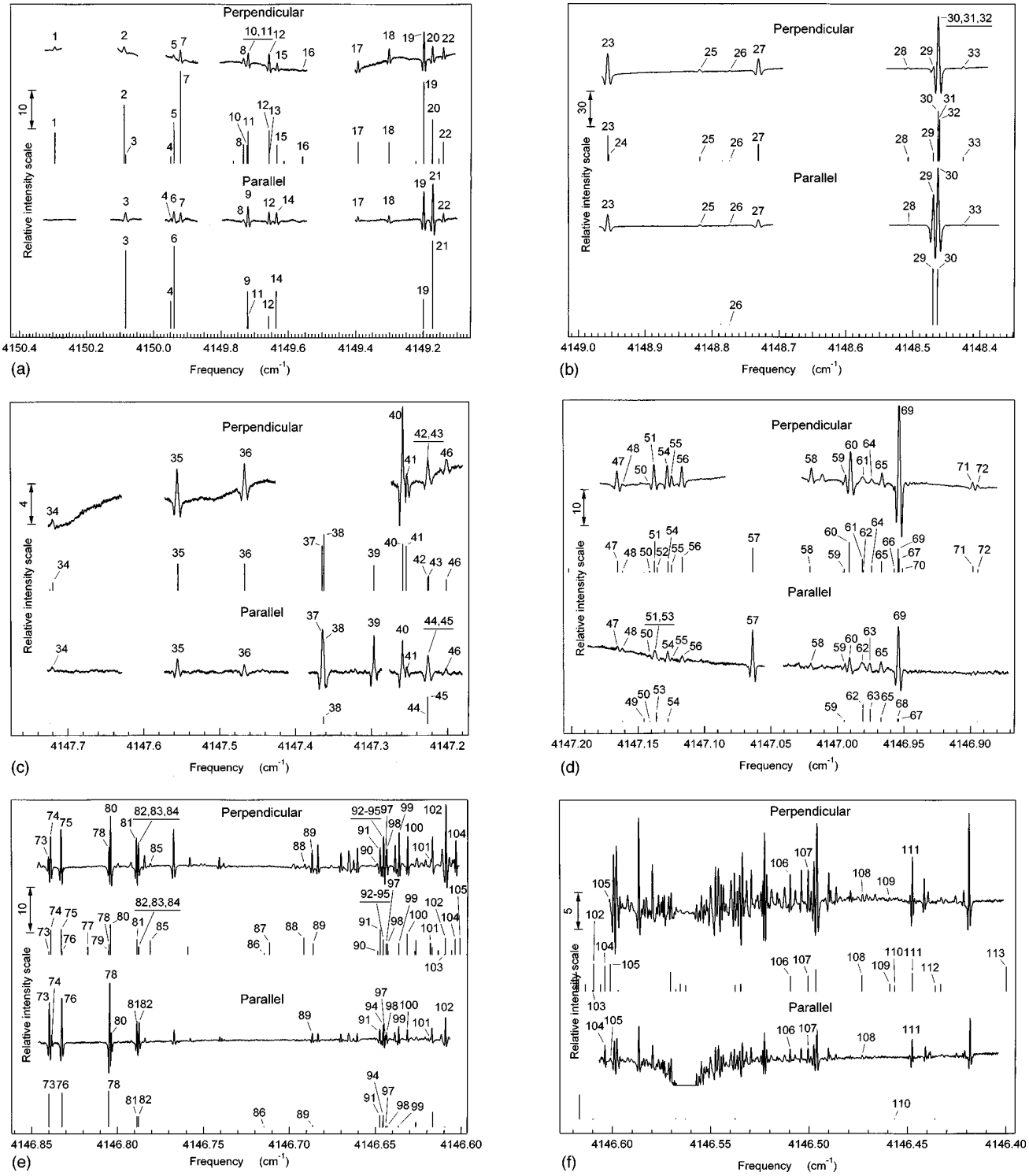

FIG. 4. Observed spectral lines compared with the theoretical, in which frequencies are calculated from the energy diagrams of Fig. 5. The radio frequencies used for the tone-burst-modulation for each figure were 120, 120, 120, 60, 13, 13, 13, 60, 120, 120, and 120 MHz, respectively, in the order of high to lower frequency of infrared. Spectra taken by laser radiation with perpendicular and parallel polarizations with respect to the *c* axis of the hcp lattice are shown in the same figure. The scale for the relative intensity in each figure is the same although it differs widely for different figures. The different rf frequencies were used because of the variety of linewidths of the observed spectrum. Spectral trace in each figure is stitched from multiple scans each spanning 0.09 cm^{-1}. The traces have gaps where no transition was observed. The numbering of the spectral lines is the same as in Table I.

splitting also holds between the IP and OP pairs. The splitting parameter for the antisymmetric excited state was found to be smaller than that for the symmetric state by about 5% for the reason that will be discussed later in Sec. VI B. We thus obtained the first approximate relative energies for the four groups of nine split levels corresponding to the vibrationally excited states IP-*s*, IP-*a*, OP-*s*, and OP-*a*. Since the orientation-dependent EQQ, CS, and non-CS interactions do

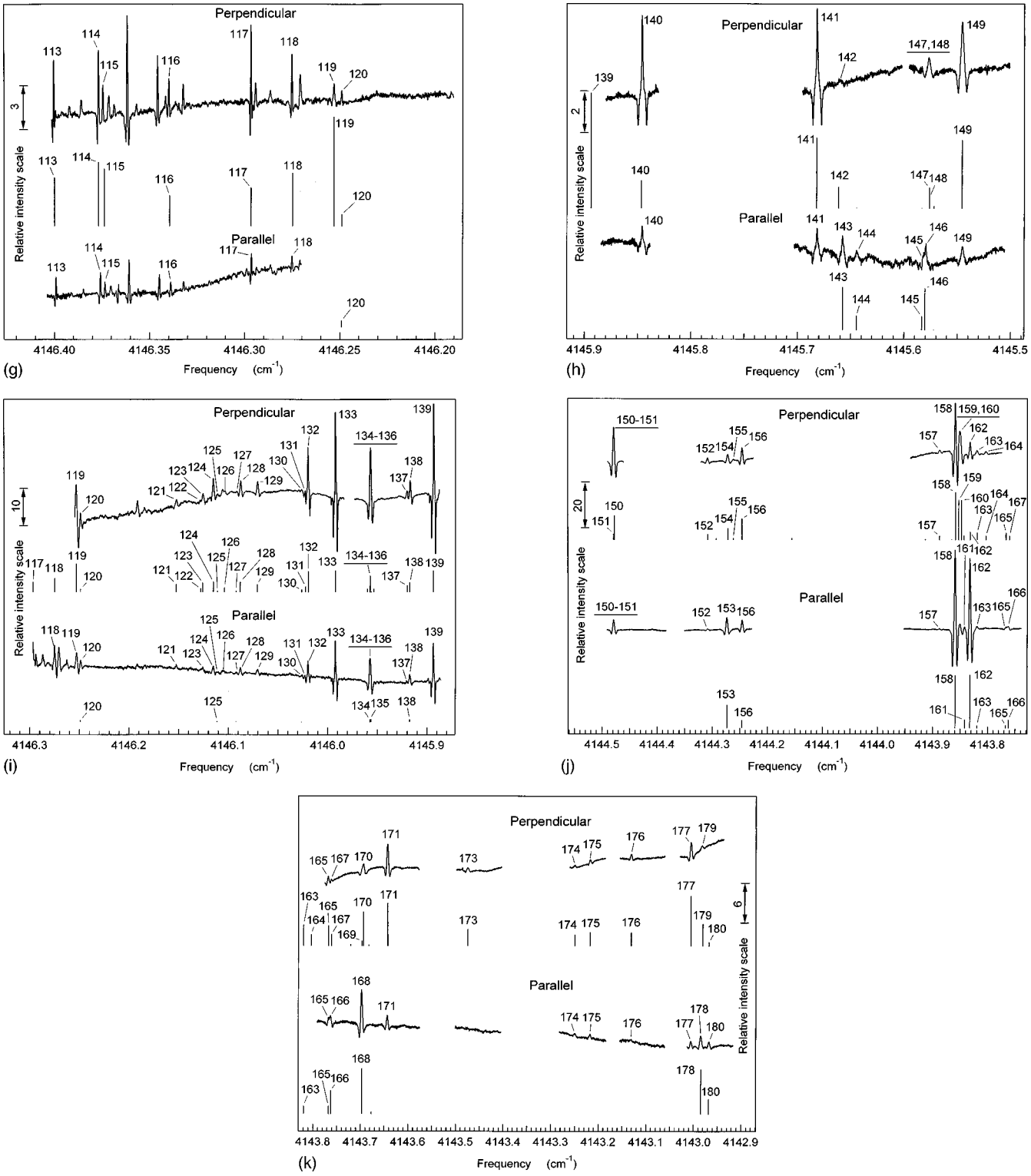

FIG. 4. (*Continued*).

not change the center of gravity of the energy levels much, we first assumed the energy difference between the center of gravity of each of the four groups and that of the ground-state pair levels to be equal to the energy of the single-molecule $Q_1(1)$ transition. We then shifted the antisymmetric levels upward and symmetric levels downward by about the same amount. This shift corresponds to the hopping of the $v=1$ vibron between the ortho-H_2 of the pair, known to be $0.2-0.3\ \mathrm{cm}^{-1}$. These first sets of approximate energy levels in the excited states allowed us to assign more spectral lines using observed linewidths, relative intensities, and laser polarization dependences. Each time a new line was assigned, an energy level in the excited state was fixed which in turn led to assignments of other transitions sharing the level. The new assignments revised the scaling factor of Γ and the shift of the *a* and *s* states, and the scaling was gradually abandoned as more spectral lines were assigned. This procedure was repeated several times until all observed lines

TABLE I. Observed $Q_1(1)$ spectral lines that are due to the nearest neighbor (NN) and next nearest neighbor (NNN) ortho-H_2 pairs. IP stands for NN in-plane pair. OP stands for NN out-of-plane pair. *a* is for antisymmetric vibrational state, *s* for symmetric. The numbering of lines is the same as in Fig. 4. The values of the observed-minus-calculated frequencies were calculated from the energy diagrams in Fig. 5 and simply indicate the consistency of spectral lines satisfying various combination differences rather than a result of a fit to a theoretical model as in an ordinary spectroscopic analysis.

Transition							Transition						
No.	Pair	$v=1$, F,M	$v=0$, F,M	Observed (cm^{-1})	Obs.−cal. (10^{-4} cm^{-1})	HWHM (MHz)	No.	Pair	$v=1$, F,M	$v=0$, F,M	Observed (cm^{-1})	Obs.−cal. (10^{-4} cm^{-1})	HWHM (MHz)
1	IP	$a20$	11_+	4150.2944	0	195.7	49	OP	$s22_+$	11_+	4147.1462	+7	
2	IP	$a20$	00	4150.0880	−5	199.1	50	NNN	$a22_+$	21_-	4147.1415	+2	27.4
3	OP	$a20$	00	4150.0841	0	194.8	51	NNN	$a22_+$	21_+	4147.1377	0	28.5
4	OP	$s20$	11_+	4149.9497	0	138.4	52	IP	$s22_-$	11_-	4147.1377	+21[a]	
5	IP	$s20$	11_+	4149.9405	+4	121.2	53	IP	$s22_-$	11_+	4147.1377	+15[a]	
6	IP	$s20$	11_-	4149.9400	+5	151.9	54	NNN	$s20$	11_+	4147.1278	+2	32.4
7	OP	$s20$	11_-	4149.9208	−3	128.9	55	NNN	$s20$	11_-	4147.1247	−2	34.0
8	IP	$s20$	00	4149.7343	0	122.9	56	OP	$s22_+$	11_-	4147.1169	0	27.2
9	IP	$a22_+$	21_+	4149.7201	−16	93.5	57	OP	$s22_-$	10	4147.0640	0	17.3
10	IP	$a22_+$	21_-	4149.7201	−34[a]	88.0	58	IP	$s22_+$	00	4147.0206	0	27.8
11	OP	$a22_-$	21_+	4149.7201	+1	88.0	59	NNN	$a00$	21_-	4146.9949	0	25.9
12	OP	$a22_+$	21_-	4149.6581	0	86.3	60	NNN	$a00$	21_+	4196.9914	+1	34.1
13	OP	$a20$	22_+	4149.6581	+8[a]		61	IP	$a20$	20	4146.9821	+6	97.5
14	IP	$a22_-$	21_-	4149.6363	0	97.7	62	OP	$a20$	20	4146.9817	+9	117.6
15	IP	$a22_-$	21_+	4149.6344	−1	74.6	63	IP	$a10$	11_+	4146.9762	+9	44.5
16	OP	$a20$	22_-	4149.5583	−2	107.1	64	IP	$a10$	11_-	4146.9753	+6	40.5
17	IP	$s22_+$	21_-	4149.3944	0	73.1	65	OP	$a10$	11_-	4146.9677	+4	26.2
18	IP	$s22_-$	21_+	4149.3024	0	70.4	66	NNN	$s11_-$	21_-	4146.9581	+6[a]	
19	OP	$a00$	21_-	4149.1996	0	60.7	67	NNN	$s11_-$	21_+	4146.9545	+6[a]	
20	IP	$a00$	21_-	4149.1744	0	73.2	68	NNN	$s11_+$	21_-	4146.9545	−4[a]	
21	IP	$a00$	21_+	4149.1727	+1	86.5	69	OP	$s22_+$	10	4146.9545	−3	16.5
22	IP	$a10$	21_+	4149.1417	+2	54.4	70	NNN	$s11_+$	21_+	4146.9499	−14[a]	
23	IP	$a11_+$	21_-	4148.9558	0	60.9	71	NNN	$s10$	21_-	4146.8983	0	29.0
24	IP	$a11_-$	21_+	4148.9558	+13[a]		72	NNN	$s10$	21_+	4146.8947	0	27.7
25	OP	$s10$	21_-	4148.8184	0	70.3	73	OP	$a22_-$	22_-	4146.8399	+1	12.9
26	OP	$s10$	21_+	4148.7738	−1	39.2	74	IP	$a22_+$	22_+	4146.8385	−2	14.4
27	IP	$s00$	21_-	4148.7313	0	80.3	75	IP	$a22_-$	22_-	4146.8326	0	15.2
28	OP	$s11_-$	21_-	4148.5081	0	71.1	76	OP	$a22_+$	22_+	4146.8326	+3	14.2
29	OP	$s11_+$	21_-	4148.4704	0	40.2	77	OP	$a11_-$	11_+	4146.8173	0	69.8
30	OP	$s11_-$	21_+	4148.4638	+2	49.5	78	OP	$a10$	10	4146.8048	−4	14.5
31	IP	$s11_-$	21_+	4148.4638	+3[a]	48.4	79	NNN	$a22_-$	00	4146.8048	−2[a]	
32	IP	$s11_+$	21_-	4148.4638	+24[a]	48.4	80	IP	$a10$	10	4146.8039	−2	12.2
33	OP	$s11_+$	21_+	4148.4260	+1	48.6	81	OP	$a11_-$	11_-	4146.7890	+3	10.3
34	NNN	$a20$	21_+	4147.7200	−2	68.6	82	OP	$a11_+$	11_+	4146.7878	0	14.8
35	IP	$a22_+$	11_+	4147.5560	+5	36.7	83	IP	$a11_+$	11_+	4146.7878	0[a]	15.5
36	IP	$a22_-$	11_-	4147.4677	0	36.7	84	IP	$a11_-$	11_-	4146.7878	+1[a]	15.5
37	OP	$a22_-$	00	4147.3653	−1	29.8	85	NNN	$a22_+$	00	4146.7809	0	20.1
38	NNN	$a20$	00	4147.3636	+2	51.0	86	NNN	$a11_-$	10	4146.7148	0	41.2
39	IP	$a22_-$	10	4147.2972	+1	21.4	87	NNN	$a11_+$	10	4146.7117	0	45.4
40	OP	$a22_+$	00	4147.2592	+2	24.3	88	OP	$a21_+$	21_-	4146.6912	−6	29.7
41	OP	$s22_-$	11_+	4147.2547	0	41.0	89	NNN	$a20$	20	4146.6870	+5	12.4
42	NNN	$a20$	22_+	4147.2264	+9[a]	49.9	90	NNN	$a11_-$	11_+	4146.6494	+8	35.4
43	IP	$s22_+$	11_+	4147.2264	0[a]	49.9	91	OP	$a21_+$	21_+	4146.6476	+3	15.1
44	OP	$s22_-$	11_-	4147.2258	−3[a]	52.9	92	IP	$a21_+$	21_+	4146.6455	0[a]	14.1
45	IP	$s22_+$	11_-	4147.2258	0	52.9	93	IP	$a21_-$	21_-	4146.6455	0[a]	14.1
46	NNN	$a20$	22_-	4147.2021	−2	54.7	94	OP	$a21_-$	21_-	4146.6455	0	12.5
47	NNN	$a22_-$	21_-	4147.1654	0	28.9	95	NNN	$a11_+$	11_+	4146.6455	0[a]	14.1
48	NNN	$a22_-$	21_+	4147.1618	0	25.8	96	NNN	$a11_-$	11_-	4146.6455	−4[a]	

TABLE I. (*Continued*).

Transition.							Transition						
No.	Pair	$v=1$, F,M	$v=0$, F,M	Observed (cm^{-1})	Obs.−cal. (10^{-4} cm^{-1})	HWHM (MHz)	No.	Pair	$v=1$, F,M	$v=0$, F,M	Observed (cm^{-1})	Obs.−cal. (10^{-4} cm^{-1})	HWHM (MHz)
97	NNN	$a22_-$	22_-	4146.6444	+5	7.8	139	OP	$s10$	22_-	4145.8938	0	10.4
98	NNN	$a22_+$	22_+	4146.6438	+8	9.8	140	IP	$s00$	22_+	4145.8459	−6	19.1
99	NNN	$a10$	10	4146.6366	0	9.2	141	OP	$s11_-$	22_+	4145.6818	−5	19.8
100	NNN	$s22_-$	10	4146.6317	0	10.2	142	IP	$s11_-$	22_-	4145.6606	−10[a]	
101	IP	$s10$	11_-	4146.6182	0		143	IP	$s11_+$	22_-	4145.6578	+1	31.5
102	NNN	$a21_-$	21_-	4146.6095	0	14.4	144	OP	$s11_+$	22_+	4145.6442	−4	
103	NNN	$a21_+$	21_+	4146.6095	−5[a]		145	OP	$s11_-$	22_-	4145.5832	−3	
104	NNN	$s22_+$	10	4146.6038	0	8.9	146	IP	$s11_-$	22_+	4145.5801	−4	
105	OP	$a21_-$	21_+	4146.6009	−1		147	IP	$s11_+$	22_+	4145.5769	+3	35.6
106	IP	$s22_+$	22_+	4146.5096	0	10.9	148	NNN	$a21_+$	20	4145.5769	+6[a]	
107	IP	$s22_-$	22_-	4146.5006	+1	11.6	149	OP	$s11_+$	22_-	4145.5456	−2	44.0
108	NNN	$a00$	22_-	4146.4731	−3		150	IP	$a21_-$	11_+	4144.4784	+9	50.0
109	NNN	$s11_-$	22_+	4146.4593	+1		151	IP	$a21_+$	11_-	4144.4784	−3[a]	40.8
110	NNN	$s11_+$	22_+	4146.4572	+6		152	IP	$a21_+$	10	4144.3085	+4	43.5
111	IP	$s10$	10	4146.4477	0	8.0	153	IP	$a21_+$	00	4144.2738	+3	61.2
112	NNN	$s11_-$	22_-	4146.4351	−9		154	IP	$a21_-$	00	4144.2722	+5	67.3
113	NNN	$s10$	22_+	4146.4000	0	9.5	155	OP	$a22_-$	20	4144.2615	0	
114	NNN	$s10$	22_-	4146.3765	−3	13.7	156	OP	$a21_-$	00	4144.2463	−1	52.6
115	OP	$a00$	22_+	4146.3741	+3	16.6	157	OP	$s21_+$	11_+	4143.8879	0	42.1
116	IP	$a10$	22_-	4146.3396	0	18.2	158	OP	$s21_+$	11_-	4143.8595	+2	39.9
117	IP	$s11_-$	11_-	4146.2965	−2	13.8	159	IP	$s21_+$	11_-	4143.8528	−3	66.2
118	OP	$a00$	22_-	4146.2753	+3	17.9	160	IP	$s21_-$	11_+	4143.8496	+12	73.0
119	NNN	$a21_+$	00	4146.2532	0	35.7	161	IP	$a21_-$	22_-	4143.8421	+3	
120	NNN	$a21_-$	00	4146.2491	0	18.4	162	OP	$s21_-$	11_+	4143.8325	0	39.6
121	IP	$a11_-$	22_-	4146.1525	1	35.0	163	OP	$a21_-$	22_+	4143.8198	+1	70.0
122	NNN	$a22_-$	20	4146.1287	+6	66.4	164	OP	$s21_-$	11_-	4143.8038	−1	80.4
123	IP	$s11_-$	10	4146.1259	−2	32.7	165	OP	$a21_+$	22_-	4143.7669	−3	53.5
124	NNN	$a21_+$	22_+	4146.1154	+1	19.7	166	IP	$a21_+$	22_+	4143.7627	+2	63.0
125	NNN	$a21_-$	22_+	4146.1113	+1		167	IP	$a21_-$	22_+	4143.7610	+3	
126	NNN	$a22_+$	20	4146.1040	0	52.3	168	OP	$a00$	20	4143.6968	−5	79.7
127	NNN	$a21_+$	22_-	4146.0918	−3	19.0	169	OP	$s21_+$	10	4143.6968	−4[a]	
128	NNN	$a21_-$	22_-	4146.0879	−1	23.8	170	IP	$a00$	20	4143.6931	−5	104.4
129	IP	$a11_+$	22_+	4146.0710	0	30.4	171	IP	$s21_-$	00	4143.6426	0	76.8
130	NNN	$s21_+$	10	4146.0265	0		172	OP	$s21_-$	10	4143.6426	+8[a]	
131	NNN	$s21_-$	10	4146.0227	0	23.1	173	IP	$a11_+$	20	4143.4750	0	95.6
132	IP	$s21_+$	21_+	4146.0203	+4	14.1	174	IP	$s00$	20	4143.2505	0	124.5
133	OP	$s10$	22_+	4145.9927	+1	9.4	175	IP	$s21_+$	22_-	4143.2181	+1	
134	NNN	$s21_-$	11_+	4145.9576	+11[a]		176	IP	$s21_-$	22_+	4143.1313	−3	81.2
135	NNN	$s21_+$	11_-	4145.9576	0		177	OP	$s11_-$	20	4143.0059	+1	69.6
136	NNN	$a00$	20	4145.9576	0		178	IP	$s11_-$	20	4142.9849	+4	124.5
137	NNN	$s11_-$	20	4145.9202	0	50.2	179	IP	$s11_+$	20	4142.9825	+19	
138	NNN	$s11_+$	20	4145.9176	0	22.6	180	OP	$s11_+$	20	4142.9680	−1	71.2

[a] Spectral lines overlapping with stronger lines.

were assigned. During this process, we noticed that the ground-state splitting of our crystals was smaller than that of microwave work. This point will be discussed further in Sec. VI A.

All observed spectral lines, which are far from the congested central region, i.e., those from 4150.3 to 4148.4 cm^{-1} at the high-frequency side and those from 4144.5 to 4142.9 cm^{-1} at the low-frequency side were assigned to transitions of NN pairs. This enabled us also to assign many NN pair spectral lines in the central region. We then proceeded to

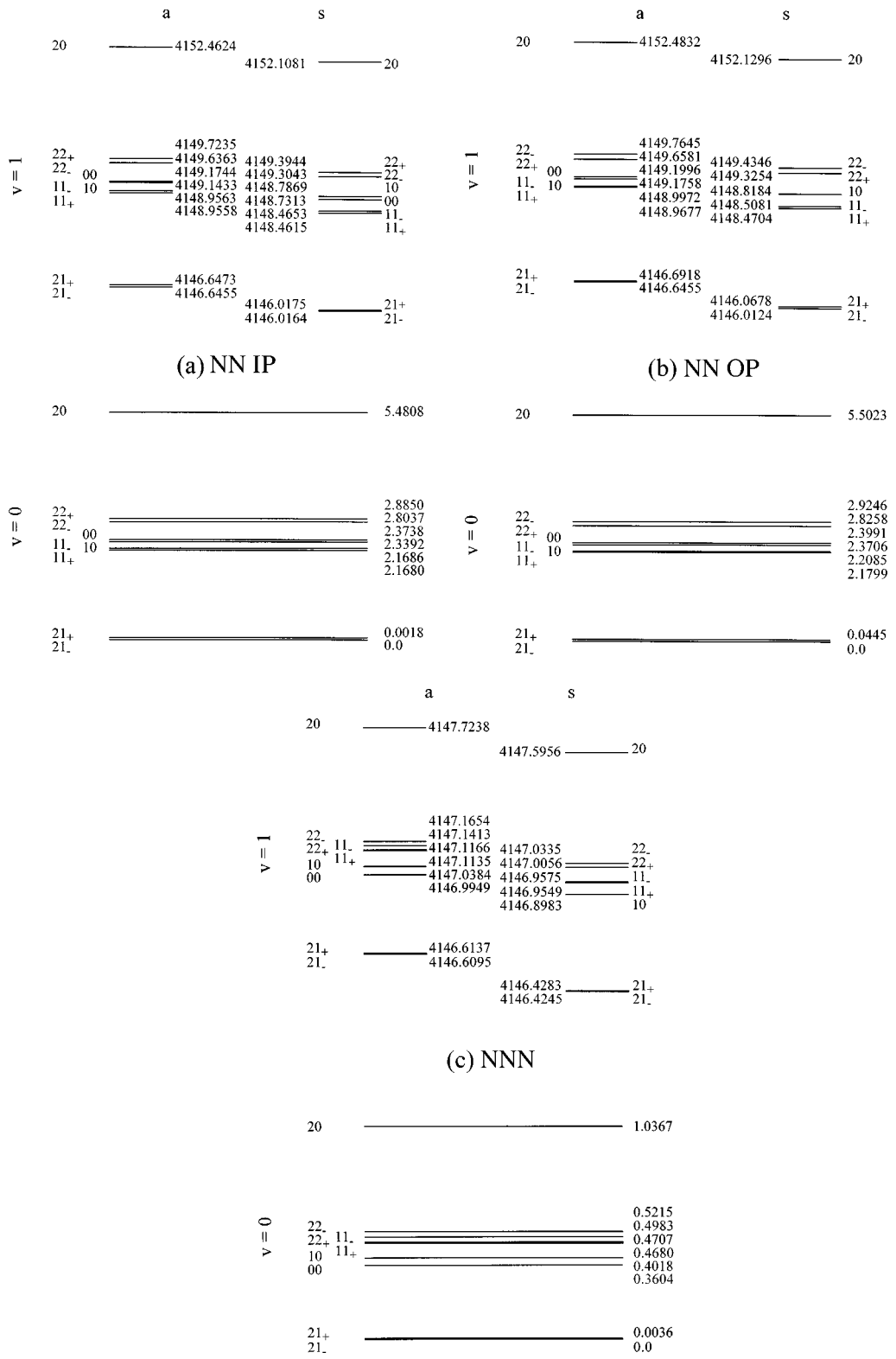

FIG. 5. Energy level diagrams of (a) nearest-neighbor (NN) in-plane (IP), (b) NN out-of-plane (OP), and (c) next-nearest neighbor (NNN) ortho-H_2 pair in para-H_2 crystals. Unit is in wave number. Values for all levels were calculated from the observed infrared spectrum. Levels are shown to scale except for the separation between the $v=1$ and $v=0$ states. Energy scales are the same also across three figures except for that of the NNN pair that has been magnified by a factor of 5.

assign transitions of NNN pair from the spectral lines that had been left unassigned using similar procedure as for NN pairs. Because of the R^{-5} dependence of the EQQ interaction, the pair splitting for the NNN pair is less than one fifth of that for the NN pairs. The splitting of the symmetric and antisymmetric states is also much lower. In assigning those crowded spectral lines, theoretical relative intensities, polarization dependences, and linewidths reported by Hardy *et al.*[21,22] were indispensable. We often relied on the *mirror effect* in which the *mirror* transitions $|F',M'\rangle_{r'} \leftarrow |F,M\rangle_r$

and $|F,M\rangle_r \leftarrow |F',M'\rangle_{r'}$ appear symmetrically with respect to the single-molecule $Q_1(1)$ frequency, with similar linewidths, intensities, and polarization dependences.

The polarization dependences are not always followed strictly due to the birefringence of some CaF_2 and sapphire windows used in the experiment. Even using sapphire windows with the c axis cut normal to the plane, a slight bend of the laser radiation affected polarization dependences. Another degradation of the polarization dependence was caused by the finite size of the laser radiation, which made part of the beam not strictly aligned with respect to the c axis of the crystal because of the cylindrical shape of the crystal cell.

Eventually all spectral lines except those in the highly congested central region over one wave number from 4147.1 to 4146.1 cm^{-1} have been assigned. The unassigned lines in this region are thought to be due to ortho-H_2 pairs farther separated than the NNN pair and ortho-H_2 clusters starting from trimers.[54] For the first 0.2% crystal studies with CCL, we observed some weak features near the NN-s $|1,1\rangle_{\pm} \leftarrow |2,1\rangle_{\mp}$ and $|2,1\rangle_{\pm} \leftarrow |1,1\rangle_{\mp}$ transitions. They are not pair transitions from their frequency positions. We ascribe these to trimer transitions, with a third ortho-H_2 molecule close by a pair perturbing the $|F,M\rangle$ levels. These spectral lines are complicated since there are many different configurations for trimers.[54]

V. RESULTS

Assigned transitions are listed in Table I. Energy levels determined from observed frequencies for NN IP, NN OP, and NNN pair are shown in Figs. 5(a)–5(c), respectively. For many cases, more than one transition sharing the same level was observed. Weighted averages of measured values were used to determine energy levels for such cases, with weight reflecting the accuracy of measuring a transition. For example, if a transition is strong, sharp, and close to a strong reference, it was given the largest weight in averaging. Weak lines, broad lines, or lines overlapping with other strong lines were not used in the average. The values of the observed-minus-calculated frequencies listed in Table I were calculated from the energy diagrams and simply indicate the consistency of spectral lines satisfying various combination differences rather than a result of a fit to a theoretical model as in ordinary spectroscopic analysis. Most of observed spectral lines are given in Fig. 4. In these figures, the calculated transition frequencies and intensities for both polarizations are included for easy comparison with the observed spectrum.

The measured linewidths for most of the assigned transitions are listed in Table I. To measure the linewidth from the tone-burst spectral line shape, a least-square fit to Lorentzian profile was applied with the following form:

$$I_0\left(\frac{2}{[(\nu-\nu_0)/\gamma]^2+1}-\frac{1}{[(\nu-\nu_0+\nu_{\rm tb}/\gamma]^2+1}-\frac{1}{[(\nu-\nu_0-\nu_{\rm tb}/\gamma]^2+1}\right), \tag{11}$$

where ν_0 is the frequency of the transition, γ is the HWHM of the transition. $\nu_{\rm tb}$ is the side band frequency of the tone-burst modulation. This form is valid when the second- and higher-order harmonics of the tone burst modulation are negligible as in our system. Both Gaussian and Lorentzian line profiles were tried for the fitting and the Lorentzian gave an overall better fit to the experimental line profile. The pure Lorentzian form was adopted to maintain the consistency. The uncertainty of the measured linewidths depends on the signal-to-noise ratio of the line but it is on the average 15% of the width.

The polarization dependence agreed well between the experiment and calculation as can be seen from Fig. 4. However, there exists a residual intensity leftover from one polarization to the other for reasons mentioned earlier in Sec. IV. Intensity data can be deceiving at times. The tone-burst modulation technique used in our experiment gives a second-derivative line shape and enhances sharp lines at the expense of broad ones. However, if we take this into account, the intensity data match the calculation pretty well.

VI. DISCUSSION

As mentioned earlier in Sec. IV, we have not carried out a full-fledged spectral analysis based on the interaction Hamiltonian. In the following we single out four interesting aspects of our results and discuss them semiquantitatively.

A. Lattice constant

As mentioned earlier, the observed ground-state pair levels are very close to the microwave values of Hardy *et al.*[20–22] except for a scaling factor. The factors for NN-IP, NN-OP, and NNN are 0.998 58, 0.998 78, and 0.999 08, respectively, with the microwave splitting being larger. Using the R^{-5} dependence of the EQQ splitting, their average 0.998 81 indicates that the lattice constant of our crystal was larger than that of Hardy *et al.* by 0.024%. There are two reasons for this larger lattice constant. First, the temperature of our crystal was higher than theirs. Our crystal cell was heat sunk to the helium bath at 4.2 K. However, the cell was typically at 5 K due to the radiation from the sapphire windows, while their crystal, grown in a microwave wave guide, was at 2.1 K. Second, our crystal was attached to the cell wall while theirs was freestanding.[21] Using the molar-volume formula $V(T)=V(0)+2.233\times10^{-6}T^{4.424}$,[31] the effective temperature of our crystal is estimated to be 7.5 K. Our crystal was expanded by about 0.02% in the lattice constant because it was attached to the wall.

B. Dependence of pair splitting on the vibrational state

From the energy levels given in Fig. 5, it is clear that the pair splitting increases in the excited vibrational states and that the splitting is larger in the symmetric vibrational state than in the antisymmetric state. If we neglect the small effect of the CS and non-CS interactions, we obtain the observed ratios of the EQQ splitting parameters in the excited state Γ_s, Γ_a and ground state Γ_0 as follows:

$$\frac{\Gamma_s}{\Gamma_0}=1.1217 \quad \text{and} \quad \frac{\Gamma_a}{\Gamma_0}=1.0623 \quad \text{for the IP NN pair,} \tag{12a}$$

$$\frac{\Gamma_s}{\Gamma_0}=1.1217 \quad \text{and} \quad \frac{\Gamma_a}{\Gamma_0}=1.0620 \quad \text{for the OP NN pair,} \tag{12b}$$

and

$$\frac{\Gamma_s}{\Gamma_0}=1.1331 \quad \text{and} \quad \frac{\Gamma_a}{\Gamma_0}=1.0735 \quad \text{for the NNN pair.} \tag{12c}$$

These results are approximately explained by the formulas

$$\Gamma_s = A\langle s|Q_1Q_2|s\rangle = A(\langle 1|Q|1\rangle\langle 0|Q|0\rangle + \langle 0|Q|1\rangle^2), \tag{13a}$$

$$\Gamma_a = A\langle a|Q_1Q_2|a\rangle = A(\langle 1|Q|1\rangle\langle 0|Q|0\rangle - \langle 0|Q|1\rangle^2), \tag{13b}$$

$$\Gamma_0 = A\langle 0|Q|0\rangle^2, \tag{13c}$$

where $A \equiv 6/25R^5$, and with the *ab initio* values of quadrupole matrix elements given by Karl and Poll.[53] Using $\langle 1|Q|1\rangle = 0.5370$, $\langle 0|Q|0\rangle = 0.4853$, and $\langle 1|Q|0\rangle = 0.0880$ all in atomic units, we obtain theoretical values

$$\frac{\Gamma_s}{\Gamma_0}=1.1394 \tag{14a}$$

and

$$\frac{\Gamma_a}{\Gamma_0}=1.073\,65, \tag{14b}$$

which are in reasonable agreement with the observed values. The fact that the observed ratios are smaller than the calculated suggests that the *effective* intermolecular distance of a $J=1$ pair *increases* upon vibrational excitation contrary to the case of the $J=0$ pair or $J=0-J=1$ pair where the vibrational excitation *decreases* intermolecular distances.[55,56] This may be explained as due to the fact that, at the equilibrium position, molecules sense the attractive part of the isotropic potential while they sense the sharply rising repulsive part of the anisotropic potential.[4,57] We see that the agreement is better in the NNN case when molecules in the pair are farther separated.

C. Linewidth

The linewidth of a transition in a solid involves contribution from both the homogeneous broadening due to relaxation and dephasing, and the inhomogeneous broadening due to the impurities and the crystal imperfections. As mentioned in Sec. III, Q-type transitions showed minimum inhomogeneous broadening and are the best candidates for studying the homogeneous broadening. We plot the linewidths of all the Q-type transitions in Fig. 6 as a function of $|\Delta E_{\mathrm{EQQ},v=1} - \Delta E_{\mathrm{EQQ},v=0}|$, where ΔE_{EQQ} denotes energy shift of the EQQ level from the center of gravity of the splitting. We note that all transitions show a similar small width except for the two NN $|2,0\rangle \leftarrow |2,0\rangle$ transitions. This demonstrates that the relaxation rate is less than a few MHz for all levels except the $|2,0\rangle$ level, which stands high above the rest of the levels. In their theoretical study of the linewidth of the microwave pair spectrum, Statt and Hardy[25] showed that, analogous to Einstein's formula for spontaneous emission, the uncertainty broadening due to the phonon-induced relaxation is proportional to the third power of energy difference between the initial and the final state $\Delta\varepsilon$

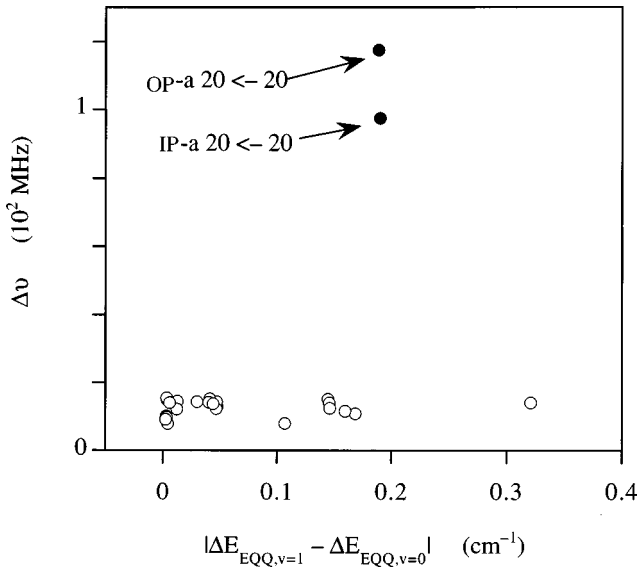

FIG. 6. Linewidths (HWHM) of all the Q-type transitions that have same values for F and M for the ground and the excited states. The horizontal axis shows the absolute values of the difference of the electric quadrupole-quadrupole interaction (EQQ) energy ΔE_{EQQ} between the excited and ground states for these transitions. ΔE_{EQQ} is defined as the relative energy of a level from the average of the nine levels. Filled circles represent Q-type transitions involving the highest NN $|2,0\rangle$ level.

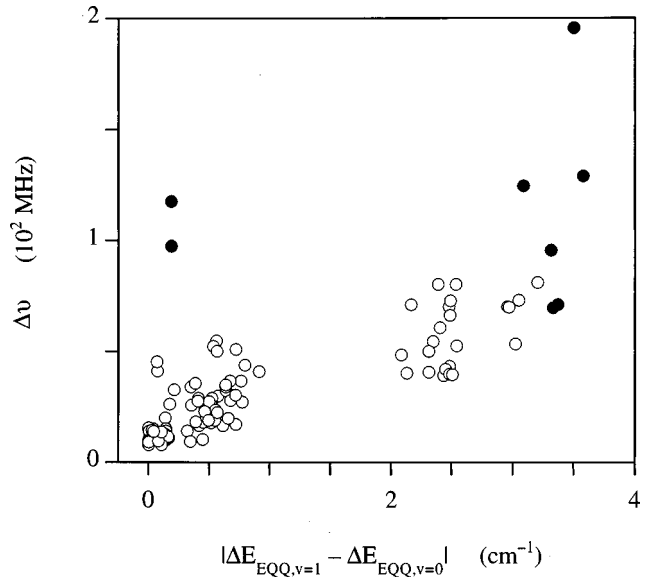

FIG. 7. Linewidth versus the absolute value of the difference of the electric quadrupole-quadrupole interaction (EQQ) energy ΔE_{EQQ} between the excited and ground state levels for all the transitions whose linewidths have been measured accurately. Open circles indicate the transitions that do not involve the NN $|2,0\rangle$ level, while filled circles indicate those that do.

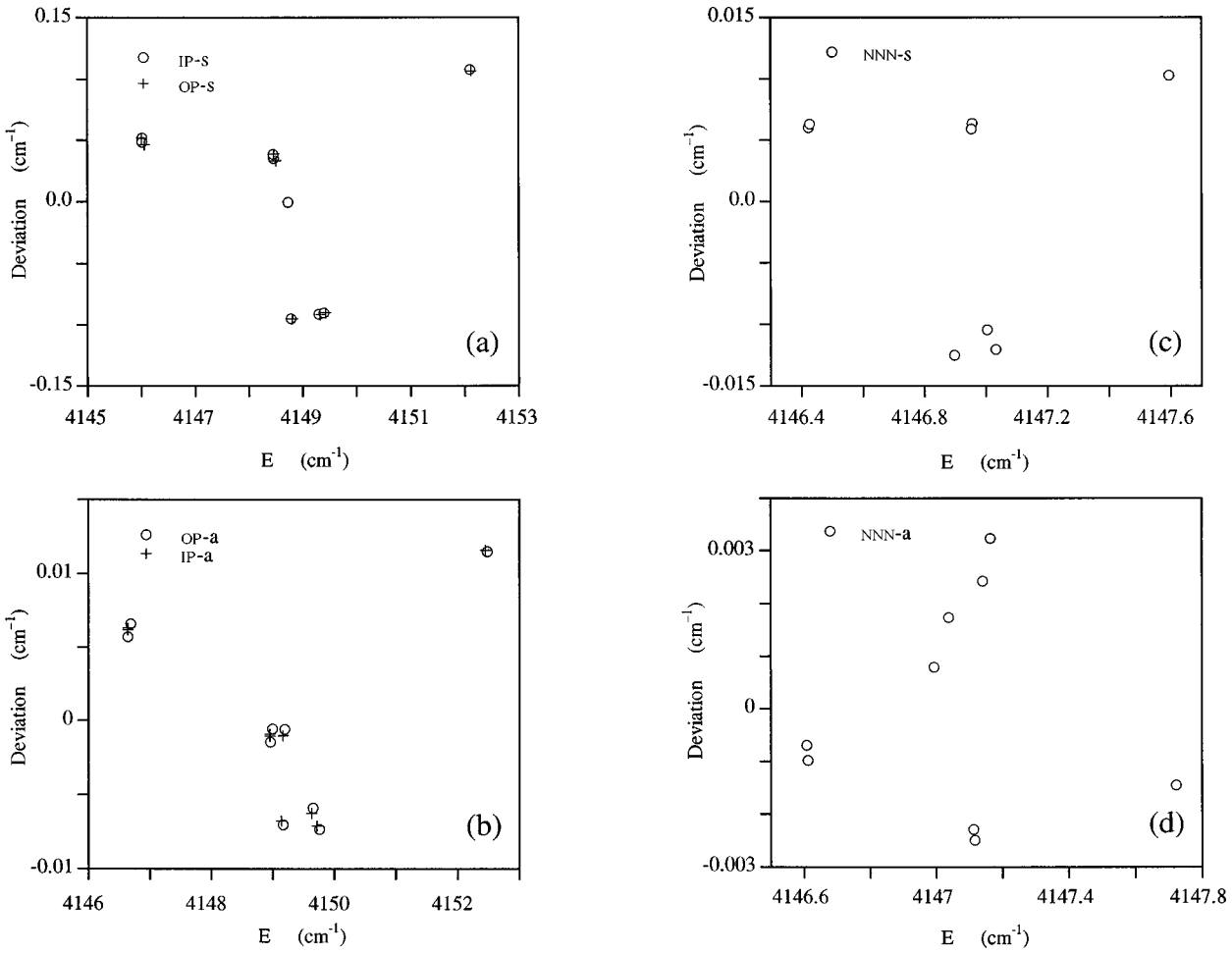

FIG. 8. Deviation from proportionality between the F, M splitting in the excited state and the ground states. The y axis represents the deviation of the measured level of an excited state from the value assuming the proportionality. E along the x axis stands for the energy levels of the excited states according to the energy diagrams in Fig. 5.

$=\varepsilon_i-\varepsilon_f$. If we assume equal relaxation matrix elements between F,M levels, we obtain the following ratios of spontaneous relaxation for the F,M levels:

$\|F,M\rangle$	Spontaneous relaxation rate in arbitrary unit
2,0	3114
$2,2_{\pm}$	254
0,0; 1,0; $1,1_{\pm}$	128
$2,1_{\pm}$	0

This explains why only $|2,0\rangle$ has homogeneous broadening that is an order of magnitude higher than the other levels.

Inhomogeneous broadening due to the EQQ interaction of the ortho pair with randomly distributed $J=1$ H_2 mainly depends on the angle-dependent interaction Hamiltonian. In Fig. 7, we plot the observed linewidth versus $|\Delta E_{\mathrm{EQQ},v=1}-\Delta E_{\mathrm{EQQ},v=0}|$. We note an approximately linear dependence excluding transitions involving the $|2,0\rangle$ level shown in black circles. The approximate linearity attests to the fact that the EQQ interaction between the pair and a farther away ortho-H_2 shifts the F,M levels in the ground state and the excited state in a similar fashion.

D. Deviation from a linear dependence

It is observed that the linear dependence for the splitting between the excited and ground states is much better followed in the antisymmetric excited state than in the symmetric one. This phenomenon is shown in Fig. 8, where the deviation from a straight linear dependence is plotted for all cases. The deviation is calculated to be the difference between the measured level of the excited state and what its value would be assuming a perfect linearity between the splitting in the excited and the ground states. The figures lead us to the following qualitative observations.

(1) For both the symmetric and antisymmetric excited states of the NN pairs, the deviations from the linearity are practically identical for IP and OP pairs. This suggests that the deviation is mainly due to the CS interactions.

(2) Between the symmetric [Fig. 8(a)] and the antisymmetric [Fig. 8(b)] excited states, the pattern of the deviations is very similar but the magnitude of the former is larger than that of the latter by a factor of 10.

(3) The deviation of the NN antisymmetric excited state and that of the NNN symmetric excited state are similar both in pattern and magnitude.

(4) The deviations of the NNN antisymmetric excited state are one order of magnitude smaller than those of the NNN symmetric state and have an inverted pattern.

VII. CONCLUSIONS

The extremely complex high-resolution infrared spectrum, observed nearly ten years ago,[29] has been assigned to the $Q_1(1)$ transitions of NN IP, NN OP, and NNN ortho-H_2 pairs by the method of ground-state combination differences using microwave results of Hardy, Berlinsky, and Harris. Observed and theoretical relative intensities, polarization dependences, and linewidths served as guides for the assignment. There are no extraneous or missing lines. The assignment has provided complete energy patterns for the six excited pair states. We leave the fitting of the observed levels by interaction Hamiltonian for future work.

ACKNOWLEDGMENTS

We would like to thank Dr. Robert Curl for lending us the CdTe modulator used in this work. We also thank Dr. Mary-Frances Jagod for the software used for data acquisition and measurement. This work was supported by the Air Force Grant No. F49620-94-1-0145.

*Present address: Department of Chemistry, Auburn University, Auburn, AL 36849-5312.

†Present address: Institute of Astrophysics and Planetary Sciences, Ibaraki University, 2-1-1 Bunkyo, Mito 310, Japan.

‡Present address: Dept. of Chemistry, Faculty of Science, Kyoto Univ., Kyoto 606-01, Japan.

§Present address: ARCH Venture Partners, L. P., 8735 W. Higgins Rd., Suite 235, Chicago, IL 60631.

‖Present address: Department of Chemistry, Michigan State University, East Lansing, MI 48824.

[1] J. C. McLennan and J. H. McLeod, Nature (London) **123**, 160 (1929).

[2] E. J. Allin, W. F. J. Hare, and R. E. MacDonald, Phys. Rev. **98**, 554 (1955).

[3] L. Pauling, Phys. Rev. **36**, 430 (1930).

[4] J. Van Kranendonk, *Solid Hydrogen, Theory of the Properties of Solid H_2, HD,* and D_2 (Plenum, New York, 1983).

[5] R. M. Dickson, T. J. Byers, and T. Oka, J. Low Temp. Phys. **102**, 241 (1996).

[6] K. Mendelssohn, M. Ruhemann, and F. E. Simon, Z. Phys. Chem. Abt. B **15**, 121 (1931).

[7] K. Schäfer, Z. Phys. Chem. Abt. B **42**, 380 (1939).

[8] J. Hatton and B. V. Rollin, Proc. R. Soc. London, Ser. A **199**, 222 (1949).

[9] F. Reif and E. M. Purcell, Phys. Rev. **91**, 631 (1953).

[10] K. Tomita, Proc. R. Soc. London, Ser. A **68**, 214 (1955).

[11] T. Nakamura, Prog. Theor. Phys. **14**, 135 (1955).

[12] N. J. Harrick and N. F. Ramsey, Phys. Rev. **88**, 228 (1952).

[13] R. W. Hill and B. W. A. Ricketson, Philos. Mag. **45**, 277 (1954).

[14] R. J. Elliott and W. M. Hartmann, Proc. Phys. Soc. London **90**, 671 (1967).

[15] A. B. Harris, L. I. Amstutz, H. Meyer, and S. M. Myers, Phys. Rev. **175**, 603 (1968).

[16] A. B. Harris, Phys. Rev. B **1**, 1881 (1970).

[17] I. F. Silvera, W. N. Hardy, and J. P. McTague, Phys. Rev. B **4**, 2724 (1971).

[18] S. A. Boggs and H. L. Welsh, Can. J. Phys. **51**, 1910 (1973).

[19] L. I. Amstutz, J. R. Thompson, and H. Meyer, Phys. Rev. Lett. **21**, 1175 (1968).

[20] W. N. Hardy and A. J. Berlinsky, Phys. Rev. Lett. **34**, 1520 (1975).

[21] W. N. Hardy, A. J. Berlinsky, and A. B. Harris, Can. J. Phys. **55**, 1150 (1977).

[22] B. W. Statt, W. N. Hardy, and R. Jochemsen, Can. J. Phys. **58**, 1326 (1980).

[23] A. B. Harris, A. J. Berlinsky, and W. N. Hardy, Can. J. Phys. **55**, 1180 (1977).

[24] S. Luryi and J. Van Kranendonk, Can. J. Phys. **57**, 307 (1979).

[25] B. W. Statt and W. N. Hardy, Can. J. Phys. **58**, 1341 (1980).

[26] R. Jochemsen, B. W. Statt, and W. N. Hardy, Can. J. Phys. **58**, 1356 (1980).

[27] T. K. Balasubramanian, C.-H. Lien, J. R. Gaines, K. N. Rao, E. K. Damon, and R. J. Nordstrom, J. Mol. Spectrosc. **92**, 77 (1982).

[28] R. A. Steinhoff, K. V. S. R. Apparao, D. W. Ferguson, K. N. Rao, B. P. Winnewisser, and M. Winnewisser, Can. J. Phys. **72**, 1122 (1994).

[29] M.-C. Chan, M. Okumura, C. M. Gabrys, L.-W. Xu, B. D. Rehfuss, and T. Oka, Phys. Rev. Lett. **66**, 2060 (1991).

[30] T. Momose, K. E. Kerr, D. P. Weliky, C. M. Gabrys, R. M. Dickson, and T. Oka, J. Chem. Phys. **100**, 7840 (1994).

[31] P. C. Souers, *Hydrogen Properties for Fusion Energy* (University of California Press, Berkeley, 1986).

[32] T. N. Antsygina, B. Y. Gorodilov, N. N. Zholonko, A. I. Krivchikov, V. G. Manzhelii, and V. A. Slyusarev, Soc. J. Low Temp. Phys. **18**, 283 (1992).

[33] T. Momose, D. P. Weliky, and T. Oka, J. Mol. Spectrosc. **153**, 760 (1992).

[34] K. E. Kerr, T. Momose, D. P. Weliky, C. M. Gabrys, and T. Oka, Phys. Rev. Lett. **72**, 3957 (1994).

[35] K. E. Kerr, Ph.D. thesis, The University of Chicago, 1995.

[36] H. M. Pickett, Appl. Opt. **19**, 2745 (1980).

[37] A. Perrin, A. N'gom, V. Dana, C. Camy-Peyret, and J.-M. Flaud, J. Mol. Spectrosc. **122**, 365 (1987).

[38] D. P. Weliky, Ph.D. thesis, The University of Chicago, 1995.

[39] V. F. Sears and J. Van Kranendonk, Can. J. Phys. **42**, 980 (1964).

[40] I. F. Silvera, Rev. Mod. Phys. **52**, 393 (1980).

[41] F. Mulder, A. van der Avoird, and P. E. S. Wormer, Mol. Phys. **37**, 159 (1979).

[42] T. Oka, J. Chem. Phys. **47**, 5410 (1967).

[43] I. F. Silvera and V. V. Goldman, J. Chem. Phys. **69**, 4209 (1978).

[44] Y. Zhang, T. Momose, and T. Oka (unpublished).

[45] T. J. Byers and T. Oka (unpublished).

[46] L. D. Landau and E. M. Lifshitz, *Quantum Mechanics, Non-Relativistic Theory* (Pergamon, New York, 1977).

[47] C. Delalande and G. M. Gale, Chem. Phys. Lett. **50**, 339 (1977).

[48] C.-Y. Kuo, R. J. Kerl, N. D. Patel, and C. K. N. Patel, Phys. Rev. Lett. **53**, 2575 (1984).

[49] I. I. Abram, R. M. Hochstrasser, J. E. Kohl, M. G. Semack, and D. White, Chem. Phys. Lett. **71**, 405 (1980).

[50] D. P. Weliky, K. E. Kerr, T. J. Byers, Y. Zhang, T. Momose, and

T. Oka, J. Chem. Phys. **105**, 4461 (1996).
[51] M. W. Crofton, M.-F. Jagod, B. D. Rehfuss, and T. Oka, J. Chem. Phys. **91**, 5139 (1989).
[52] C. M. Gabrys, D. Uy, M.-F. Jagod, T. Oka, and T. Amano, J. Phys. Chem. **99**, 15 611 (1995).
[53] G. Karl and J. D. Poll, J. Chem. Phys. **46**, 2944 (1967).
[54] H. Miyagi, Prog. Theor. Phys. **40**, 1448 (1968).
[55] R. M. Dickson, T. Momose, T. J. Byers, and T. Oka, Phys. Rev. B **57**, 941 (1998).
[56] R. M. Dickson and T. Oka, Phys. Rev. B **57**, 950 (1998).
[57] G. A. Gallup, Mol. Phys. **33**, 943 (1977).